

By the signing of this article, the publisher or recipient acknowledges the U.S. Government's right to retain a nonexclusive, royalty-free license in and to any copyright covering the article.

X-RAY SPECTROSCOPY ON TOKAMAKS

Conf-820944-5

CONF-820944--5

DE82 022242

S. von Goeler, M. Bitter, S. Cohen, D. Eames, K. Hill,
D. Hillis*, R. Hulse, J. Lenner, D. Manos, Ph. Roney, W. Roney,
N. Sauthoff, S. Sesnic**, F. Tenney, J. Timberlake

Plasma Physics Laboratory

Princeton University, Princeton, N.J. 08544

MASTER

During the last decade the X-ray spectroscopy of high temperature plasmas has witnessed a rapid development.^{1,1a,2,3,4,5} Most of the impulses have come from astrophysics, in particular, from the research on solar flares. On the other hand, the attainment of well-diagnosed, high-temperature laboratory plasmas in laser-pellet implosions and in tokamaks, has precipitated a fertile exchange between theory and experiment. Agreement and very detailed understanding has been reached for a great number of spectra with the result, that X-ray spectroscopy represents today a powerful and reliable new plasma diagnostic with important applications for fusion plasmas as well as solar flares. This paper is a short review of the experimental results from tokamaks.

DISCLAIMER

This report was prepared as part of the work sponsored by the United States Government. It is not to be distributed outside the Government. The views and opinions contained herein are those of the author and do not necessarily represent those of the United States Government. This report is the property of the United States Government and is loaned to you; it and its contents are not to be distributed outside the Government.

* On leave from Oak Ridge National Laboratory, Oak Ridge.
** On leave from the Max-Planck Institut, Garching, Germany.

I. Instrumentation

For the investigation of X-ray line radiation plane and curved crystal spectrometers are used. The curved crystal spectrometers^{6,6a} have definite advantages for high resolution work. However, since we dealt already with curved crystal spectrometer in our first lecture^{6b} on TFTR diagnostics, and since Dr. Bartiromo⁷ will present a detailed description of his instrument in another paper at this conference, we will not discuss the curved crystal spectrometer here in order to avoid repetition. We shall give, however, a brief description of the rotating plane crystal spectrometer.^{7a} This instrument has been used during the past two years on PLT for the investigation of radiation in the 5 to 25Å region. This wavelength range is called the ultra soft X-ray (USX) region and contains the K spectra of low-Z ions like oxygen or neon as well as the L spectra of medium-Z ions like titanium or iron. The USX radiation has not been studied in great detail up to now because vacuum spectroscopy is required. For wavelength longer than 26Å, gratings are better than X-ray crystals and ultraviolet spectroscopy takes over.

A schematic drawing of the rotating crystal spectrometer is shown in Fig. 1. Ultra soft X-ray radiation enters the instrument through a "see thru" valve and is made parallel by a set of Soller slots. The Soller slots consist of a stack of metal plates made out of .005" thick stainless steel shim stock separated by .010" thick spacers. The use of Soller slots in this wave length range is questionable, because reflection of radiation at glancing incidence is appreciable. Astrophysicists successfully used a series of carefully aligned photo-edged screens as collimators.⁸ Visible and ultraviolet light enters the spectrometer together with X-rays, and in order to minimize this unwanted contribution a thin foil^{8a} consisting of 10000Å parylene (C₈H₈) and

6000Å aluminum is inserted into the beam path. The aluminum keeps out most of the far ultraviolet and visible light. The thickness of the parylene is carefully tailored so as to close the transmission window of the aluminum below 73 eV (Fig. 2). The radiation which has been made parallel by the Soller slots is Bragg reflected from an X-ray crystal. The best results were obtained with thallium acid phtalate (TAP) crystals because TAP has the highest reflection coefficient.⁹ The resolution of this very crude instrument is not determined by the crystal but by the angle aperture of the Soller slots. The crystals are mounted on a shaft rotating with an angular velocity of 600 rpm. In order to measure the angle of rotation, the light beam in a LED-photodiode^{9a} combination is interrupted by a slotted plate. The photo diode current is read by a transient analyser. The radiation which is reflected from the crystal is measured by a "wide area" detector, consisting of four pairs of micro-channel plates^{10,11} in chevron configuration. The microchannel plates have a sensitive area of 2 cm x 4 cm. The current generated by the X-ray photons in the channel plates is picked up by four collector plates. The final output of the rotating crystal spectrometer consists then of the collector current vs. time (Fig. 3). Using the signals of the LED - photo detector pick up, the computer converts time into Bragg angle and Bragg angle into wavelength. Wavelength calibration is obtained in situ on the tokamak by observing line radiation from hydrogenlike ions like O VIII or NeX. The radiation from these ions, which will be discussed in more detail in the next section, can be calculated theoretically with high accuracy¹² and constitutes an excellent reference standard. An intensity calibration has not been performed yet; it can probably be obtained from synchrotron radiation storage rings. A turning point and bellows at the vacuum-vessel interface permit radial scanning.

A discussion will now be given of the line radiation emitted from tokamak plasmas in the soft (SX) and ultra soft (USX) X-ray region. The spectra will be considered in isoelectronic sequences.

II. Hydrogenlike Spectra

The spectrum of hydrogenlike oxygen (O VIII) is shown in Fig. 4. The spectrum was obtained with the rotating crystal spectrometer described in the previous section. It shows the main resonance transition ($1s - 2p$) at the wavelength 18.97\AA . This line corresponds to the Lyman α transition in hydrogen. The position of the Ly β and Ly γ lines is also indicated in Fig. 4 by arrows at a wavelength of 16.01\AA and 15.21\AA . Ly α really consists of two transitions, namely, $1s\ 2S_{1/2} - 2p\ 2P_{3/2}$ and $1s\ 2S_{1/2} - 2p\ 2P_{1/2}$. For oxygen, the $2P_{3/2}$ and the $2P_{1/2}$ level are so closely spaced that the two lines cannot be separated. For higher-Z ions, the levels are spaced further apart. Figure 5 shows an example where the two lines are nicely resolved, namely, a hydrogenlike spectrum of sulfur obtained by E. Kälné¹³ on Alcator. Another feature of the spectra which becomes prominent for the high-Z ions are dielectronic satellites. The appearance of these satellites is indicated in Fig. 5 at wavelength 4.760\AA and 4.784\AA . There are theoretical predictions for hydrogenlike satellites available;^{13a,14} however, since the satellites are much more pronounced for helium-like ions, we will defer a detailed discussion for later.

As far as diagnostic applications are concerned, the Ly α line has been used on tokamaks to measure the particle transport.^{15,16,17} Figure 6 and 7 illustrate the method which is based on the interpretation of radial emission profiles. Hydrogenlike neon (NeX) is located in the outer plasma regions; in the center of the discharge neon is in the proton-like charge state. Figure

6a shows theoretical predictions of the radial distribution of hydrogenlike Ne X ions in PLT with the multi-ionized-species-diffusion code MIST.¹⁸ The three curves assume a diffusive charge-state equilibrium where the neon transport is modeled by a diffusion term with diffusion coefficient D equal to $1 \cdot 10^4$ cm²/sec, $4 \cdot 10^3$ cm²/sec and zero, respectively. The Ly $_{\alpha}$ radiation comes from a region that is located on the inside wing of the radial profile of NeX (Fig. 6b), because the excitation energy for Ly $_{\alpha}$ is comparatively large. With transport, the Neon X ion can penetrate to the hot center of the discharge where it radiates much more intensely. The net result is an increase of the Ly $_{\alpha}$ radiation with diffusion and an inward shift of the maximum of the Ly $_{\alpha}$ emission. The experimental data clearly exhibit an inward shift (Fig. 7), which is consistent with a diffusion coefficient of approximately 10^4 cm²/sec.

Hydrogen-like lines can also be utilized for the measurement of ion temperatures from Doppler broadening. This application will figure very prominently on fusion reactors, when the electron temperature will exceed 6 keV and iron will be predominantly in the hydrogenlike charge state at the center of the discharge.

III. Heliumlike Spectra

The helium-like spectra have been investigated in great detail. This is due largely to the stimulus provided by a very important pioneering paper by Gabriel.¹⁹ A typical helium-like spectrum of oxygen (OVII) from a tokamak plasma is shown in Fig. 4 at a wavelength of 22.6Å. It consists essentially of two lines: (1) The resonance line ($1s^2 \ ^1S_0 - 1s \ 2p \ ^1P_1$) at 21.6Å and (2) the intercombination line ($1s^2 \ ^1S_0 - 1s \ 2p \ ^3P$) at 21.8Å. The heliumlike $1s - 2p$ transitions are called K $_{\alpha}$ lines. The corresponding $1s - 3p$ or K $_{\beta}$ transitions occur at 18.77Å.

The K_{α} - spectrum of heavier impurities, for example, the spectrum of iron by M. Bitter²⁰ shown in Fig. 8, exhibits a much larger variety of lines. There are three factors which bring about this profusion of lines: (1) The emergence of the forbidden line, (2) the growing importance of dielectronic satellites and (3) the prominence of inner shell transitions. We will discuss these factors now in more detail, and start with a discussion of the forbidden line.

A term diagram for the $1s - 2p$ transition of helium-like ions is shown in Fig. 9. The solid arrows indicate collisional excitation, the dashed arrows radiative transitions. The resonance transition $1S_0 - 1P_1$ is marked with the letter w. The intercombination line consists really of two transitions, namely $1S_0 - 3P_2$ and $1S_0 - 3P_1$. They are marked in Fig. 9 with the letters x and y. For oxygen the two lines are so close in wavelength that they cannot be resolved. For iron, they are well separated (Fig. 8). The transition y takes place through breakdown of LS coupling for high Z ions where as x results from a magnetic quadrupole transition. In the iron spectrum, the transition $1S_0 - 3S_1$ is very prominent. It is designated with the letter z, and carries the name "forbidden" line (F); it actually takes places as a relativistic magnetic dipole transition. For low-Z ions, like oxygen, collisional excitation from the $3S_1$ to the $3P$ level is strong enough, so that ions in the metastable $3S_1$ level decay via the $3P$ level and contribute to the intercombination line. For high-Z ions like iron, the probability for collisional transfer to the $3P$ level becomes small compared to the probability for radiative transition to the ground-state, and the forbidden line becomes very prominent.

On PLT, laser blow-off techniques²¹ permit to inject practically any impurity into the tokamak, and the emergence of the forbidden line with

increasing Z can be followed in detail. The K_{α} -spectrum of neon ($Z = 10$) has the same shape as the oxygen spectrum, and the forbidden line is very small. For magnesium ($Z = 12$) the forbidden line is stronger than the intercombination line (Fig. 10). Theoretical prediction for the intensity of lines R, I and F have been made by a number of authors, most recently by Pradhau and Shull.²² Reasonable agreement has been obtained for a solar flare spectrum of calcium,^{22a} while detailed computations²³ and measurements^{22,24} for iron have persistently shown discrepancies for the line ratios of x, y, z and w. For magnesium Pradhau²² predicts $F/I = .5$ for PLT conditions, which is lower than the experimental result shown in Fig. 10. The line ratio F/I depends on collision rates and is, therefore, used by astrophysicist as a diagnostic for the plasma density.

Let us now turn to the dielectronic satellites. They are represented in Fig. 8 by the lines t, k, r and j. There exists actually a quite large number of these satellites, which have been calculated in the classic papers by Gabriel¹⁹ and Bhalla, Gabriel and Presnyakov.²⁵ However, most of the satellites have small intensities and some occur at longer wavelength and, therefore, do not show up in Fig. 8.

The process of dielectronic recombination of heliumlike ions involves the radiationless capture of an electron and the simultaneous excitation of a K-shell electron. The result is a doubly excited lithiumlike ion. The excited ion can decay by autoionization, the inverse process. Another possibility is that the recombination process is "stabilized by" a radiative transition of the excited ion. The line radiation which is emitted in the recombination process belongs into the lithiumlike spectrum and is of the type $1s^2 nl - 1s 2p nl$. The same lines can consequently also be produced by inner shell excitation of lithiumlike ions. It so happens, that a few of the

satellites are produced predominantly by inner shell excitation while others are produced only by dielectronic recombination. The first case is represented by the satellite q, which has the spectroscopic notation $1s^2 2s^2 2S_{1/2} - 1s 2p(1P_1) 2s^2 2P_{3/2}$, and which happens to have an extremely small dielectronic capture cross section.²⁵ The intensity of this line, I_q , is then proportional to the density of lithiumlike ions in the groundstate, and in diagnostic applications this line is used to measure the number density of ions in the lithiumlike charge state. The other case, namely, where dielectronic recombination is responsible for the line excitation is represented by the satellite j which has the spectroscopic notation $1s^2 2p^2 2P_{3/2} - 1s 2p^2 2D_{5/2}$. Inner shell excitation of this line from the lithiumlike ground state $1s^2 2s^2 2S_{1/2}$ would require simultaneous excitation of two electrons which has a very low probability. A level diagram for this transition is shown in Fig. 11. Since the satellite j is produced by dielectronic recombination, its line intensity is proportional to the heliumlike ion density, as is the case for the resonance line w. However, the excitation mechanism for the two lines is completely different. The line w is excited by electrons with energy greater than the excitation energy of the line w, namely 6.7 keV. On the other hand, the satellite j is excited because of energy conservation only by electrons which have an energy of 4.7 keV, i.e., the difference between excitation energy of the lithiumlike $1s 2p^2 2D_{5/2}$ level (6.7 keV) and the ionization energy of lithiumlike ions (2.0 keV). The line ratio I_j/I_w is consequently independent of the abundance of the ion and strongly temperature dependent. The line ratio is plotted versus the electron temperature in Fig. 12 for iron. As a consequence, the theory for dielectronic recombination is in excellent agreement with the experiment.²⁰ The figure also illustrates that the line ratio I_j/I_w represents a sensitive diagnostic for the electron temperature.

The satellite β in Fig. 8 is due to the transition $1s^2 2s^2 1S_0 - 1s 2s^2 2p^1 P_1$ of berylliumlike iron. This line has similar properties as the satellite q and is excited predominantly by collisional inner-shell excitation. Besides the satellite β , there exist a large number of satellites at longer wavelength which are due to iron ions in the beryllium, boron, carbon, nitrogen, oxygen, fluorine and neonlike charge states. Extensive calculations for these satellites have been performed by Merts, Cowan and Magee.²⁶ Experimentally, these satellites have been first investigated on tokamaks by Hill et al.⁶ and have been used to determine the charge state equilibrium. A high-resolution spectrum of these satellites of chrome has been recently obtained by Platz and Ramette²⁷ and is shown in Fig. 13. The lines of the carbonlike ions (satellites 11-14) and the lines of the nitrogenlike ions are of special interest to astrophysicists²⁸, because the recombining ions have a first excited level very close to the ground state that is populated by collisions.^{29,30} The line ratio of these satellites can consequently be used as a density diagnostics which is expected to be highly sensitive in the density range encountered in tokamaks (10^{13} cm^{-3}).

The heliumlike lines and satellites are of great interest to astrophysicists and plasma physicists, because they offer so many diagnostic possibilities. We have mentioned most of diagnostic applications as we discussed the structure of the spectra. For instance, the lines w , q , β etc. are used to determine the charge state distribution. Deviations from the charge state distribution predicted by coronal equilibrium are caused by particle transport. The particle confinement time can consequently be deduced from line ratios I_q/I_w .³¹ A particularly elegant method for measuring confinement has been developed by Peacock et al.³² on Dite and exploits the forbidden lines x , y and z for diffusion measurements. Further more, the line

ratio I_j/I_w is valuable for electron temperature measurements. The most important diagnostic application for tokamaks, however, is unquestionably the determination of the ion temperature from Doppler broadening, which we will discuss now.

Figure 14 illustrates the time development of the line profile of the helium-like resonance transition w of titanium during neutral beam heating.^{6a} Neutral beam injection takes place in the time period from 300 to 450 ms. The data shown in Fig. 14 clearly exhibits a strong broadening of the line during the heating. The ion temperature actually reached a value of 5.5 keV at 412 ms. Another clearly observable feature is a shift of the centroid of the line towards shorter wave wavelength during neutral beam injection. The shift is interpreted as a Doppler shift due to toroidal rotation of the plasma. The toroidal rotation³⁴ is caused by the momentum transfer to the plasma by injected ions. (The crystal spectrometer on PDX is inclined by 16° in toroidal direction with respect to the radial line of sight.) The Doppler shift seen in Fig. 14 translates into a toroidal velocity of 1.10^7 cm/sec.

Doppler broadening is not the only process that determines the line width lines in the X-ray region. Because of the large transition probabilities of the X-ray lines and the resulting short lifetimes of the excited states, natural line broadening gives a noticeable contribution. Since Doppler broadening gives rise to a Gaussian line profile while natural broadening leads to a Lorentzian profile, the resulting line shape will be a convolution of the two, namely a Voigt function.³⁵ There is still another process which contributes to the broadening of many X-ray lines, a process which may be called dielectronic broadening and has been discovered only recently,^{36,24}. This type of broadening is caused by a blend of unresolved satellites that are

produced by dielectronic recombination when electrons are captured into orbits with higher main quantum number $n = 3, 4, 5...$ etc. A typical example for this transition is the satellite d_{13} , which clearly shows up in the iron spectrum shown in Fig. 8. The satellite d_{13} represents the same transition as the dielectronic satellite j except that one of the two excited electrons is in the $3p$ state instead of the $2p$ state (Fig. 11). The satellite d_{13} is not the only $n = 3$ satellite; there are many $n = 3$ satellites which form an unresolvable blend marked A and B in Fig. 8. For the higher quantum numbers, n , the electron orbits quite far out from the core, and, as a result, the $1s - 2p$ transition energy for the doubly excited lithiumlike ion is almost identical with the transition energy of the heliumlike ion. Therefore, the $n \geq 4$ satellites form blends of lines that approach the resonance line w in a series limit. This characteristic feature of the $n \geq 3$ satellites is illustrated in Fig. 15 which presents theoretical calculations of the unresolved satellites by Bely-Dubau et al.³⁶ A comparison of the theoretical predictions with the experiment by Bitter et al.²⁴ is shown in Fig. 16. The unresolved $n \geq 3$ satellites do not only contribute to line broadening, but they also cause an increase of the effective intensity of the resonance line w . The relative contribution to the line intensity, a shows up for example in Fig. 12, where it is crucial for establishing a definite agreement between experiment and theory.

IV. The L-Spectra

Up to now, we have considered transitions of the type $1s - 2p$ which involve excitation of an electron from the K shell and which are consequently named K spectra. We now want to discuss transitions between the $n = 2$ and $n = 3$ shell, the so-called L-spectra. These tend to fall into the ultra soft

X-ray region (5...25Å), and involve, because of the 25Å limit, only atoms with Z larger than 20.

Figure 17 shows an L-spectrum of iron, which has been measured with the rotating crystal spectrometer on PLT. The particular tokamak discharge has a stainless steel limiter and the spectrum is really from 305 stainless steel (Fe, Cr, Ni). However, chromium and nickel are present only in small percentages and most of the lines have been correctly attributed to iron. Unique line identification for iron, chromium and nickel has been obtained with laser blow-off techniques and with the help of Ref. 37, 38, and 39. The relevant transitions have been indicated above the spectrum. There occur basically three types of transitions: $2p - 3s$, $2p - 3d$ and $2s - 3p$. Each in turn consists of an array of lines, which is produced by various alignments of the angular momentum and the spin. For neonlike iron (FeXVIII), the three arrays are located approximately at 17Å, 15Å and 13.8Å. For the fluorinelike charge state FeXVII, the three arrays are shifted to somewhat shorter wavelength. The pattern repeats down to the lithiumlike charge state. In present day tokamaks with central electron temperatures in the range of 1 to 2 keV, the lithiumlike iron lines are emitted from the central plasma region, while the neonlike lines come from the outer rim of the plasma. Figure 18 shows the chord integrated emission of some of the major iron L-lines as a function of radius. Radial profile of the charge states can be deduced from these data, which, for the particular discharge, do not deviate far from the prediction from coronal equilibrium. For iron, the lines from the lithiumlike and the neonlike charge states have about comparable intensity in PLT discharges. For elements with smaller Z, the higher charge states are favored. This is illustrated in Fig. 19 which shows a titanium L spectrum obtained with the help of laser blow-off techniques.²¹ The lithiumlike lines

indicated in Fig. 19 by arrows. For elements with a higher Z than iron, on the other hand, the lower charge state dominate. Figure 20 shows a germanium L spectrum. The ionization potential of neonlike germanium is 3000 eV, and fluorinelike germanium is practically absent in this particular, relatively cool PLT discharge. The spectrum shown in Fig. 20 is, therefore, purely neon-like. The line at 10.02\AA is a forbidden magnetic quadrupol transition, which has been analyzed for iron by Klapisch et al.⁴⁰

The L spectra consist of a very large number of transitions and are therefore more complicated than the K spectra. The spectra are also of interest to astrophysicists and spectra similar to the one shown in Fig. 17 have been obtained from the solar corona by McKenzic et al.⁴¹ Tokamak experiments permit to check theoretical predictions for these lines. Dielectronic recombination seems to be of less importance. The true diagnostic potential of the L lines might lie in the fact that the radiation intensity is quite large so that fast changing plasma conditions can be investigated and recorded.

References

References 1 to 5 are review articles on X-ray spectroscopy.

- ¹A.H. Gabriel and C. Jordan: Case Studies in Atomic Collision Physics 2, p. 211 (1972).
- ^{1a}R. McWhirter in "Course on Plasma Diagnostics and Data Acquisition Systems" Varenna, Ed. H. Eubank and E. Sindoni, Editrice Compositori, Bologna, p.178 (1978)
- ²R.D. Cowan: "The Theory of Atomic Structure and Spectra" University of California Press, (1981).
- ³J. Dubau and S. Volonte: Rep. Prog. Phys. 43, 199 (1980).
- ⁴C. De Michelis and M. Mattioli: Nucl. Fusion 21, p.677 (1981).
- ⁵N.J. Peacock in "Applied Atomic Collision Physics" Vol. II (to be published).
- ⁶K. Hill et al.: Phys. Rev. A19, p.1770 (1979).
- ^{6a}M. Bitter et al. in "Proc. 6th Gut. Symposium on Temperature" Washington, D.C. (1982) also Princeton Report PPPL-1897 (1982).
- ^{6b}S. von Goeler et al: "X-ray Diagnostics for TFTR", lecture at this conference.
- ^{7a}D. Eames: PH.D dissertation, Princeton University (1980).
- ⁷R. Bartiromo: "Crystal Spectroscopy" lecture at this conference.
- ⁸Astrophysicists [photo edged screens].
- ^{8a}Le Bow Co., Goleta, CA. 93017, USA.
- ⁹A. Burek (Los Alamos on Report LA-UR 75-1593/1975)
- ^{9a}LED - Photo discs combination.
- ¹⁰Galileo Electro Optics Corp., Sturbridge Man., 01518, USA.
- ¹¹Landouer Nucl. Instr.

- ¹²J. Garcia and J. Mack: Journ. Opt. Soc. America 55, p.654 (1965).
- ¹³E. Kalne et al.
- ^{13a}Hydrogenlike iron, titanium Dubau, ? Clark.
- ¹⁴L.A. Vainshtein and U.T. Safronova: Atomic Data and Nucl. Data Table 21, p.49 (1978).
- ¹⁵TFR Group, J. Doyle, J. Schwab: Fontenay-aux-Roses report EUR-CEA-FC-1121.
- ¹⁶Fupmann
- ¹⁷S. von Goeler et al: Bull. APS
- ¹⁸Russel Hulse MIST - Code.
- ¹⁹A.H. Gabriel: Mon. Not. R. Soc. 160, p.99 (1972).
- ²⁰M. Bitter et al: Phys. Rev. Lett. 43, p.129 (1979).
- ²¹S. Cohen Laser Blowoff.
- ²²A. Pradhan, and J.M. Shull: The Astrophys. Journ. 249 p.821 (1981).
- ²³F. Bely - Dubau et al.: Month Not. Roy. Astron. Soc. 198, p. 239 (1982).
- ²⁴M. Bitter al al: Phys. Rev Lett. 47, p.921 (1981).
- ²⁵C.P. Bhalla, A.H. Gabriel and L.P. Presnyakov: Mon. Not. Roy. Astr. Soc. 172, p.359 (1975).
- ²⁶A. Merts.
- ²⁷TFR group, J. Dubau, M. Loulerque At. J. Phys. B: Mol. Phys. 15, p.1007 (1981).
- ²⁸Ken Phillips (private communication).
- ²⁹H.E. Mason and P.J. Storey: Mon. Not. Roy. Astron. Soc. 191, p.631 (1980).
- ³⁰U. Feldman, G.A. Doschek, R. Kreplin: Astrophys. Journ. 238, p.365 (1980).
- ³¹Brussels paper.
- ³²N. Peacock et al., Plasma Physics and Contr. Nucl. Fusion Res., Innsbruck, Vol I, p.303 (1979).
- ³³M. Bitter et al: Phys. Rev. Lett. 42, 304 (1979).

- ³⁴Sauthoff et al Innsbruck.
- ³⁵Voigt function.
- ³⁶F. Bely - Dubau, A.H. Gabriel, S. Volonte: Month. Not. Roy. Astr. Soc. 189, p.801 (1979).
- ³⁷G.E. Bromage, R.D. Cowan et al., Culham Report CLM-R 170 (1977).
- ³⁸G.E. Bromage, R.D. Cowan, B.C. Fawcett and A. Ridgeley: Journ. Opt. Soc. Am. 68, p.48 (1978).
- ³⁹Kelly Palumbo: Naval Res. Laboratory report NRL-7599 (1973).
- ^{39a}G.E. Fawcett, R.D. Cowan and R.W. Hayes: Astrophys. Journ. 187, 377 (1973).
- ⁴⁰M. Klapisch et al: Physics Lett. 69A, p.34 (1978).
- ⁴¹McKenzie.

Figure Captions

- Fig. 1 The rotating crystal spectrometer.
- Fig. 2 Transmission characteristics of the aluminum-parylene foil according to Biggs and Lighthill. μ is the absorption coefficient and d the thickness of the foil. Absorption edges occur at 73 eV and 1560 eV for aluminum and at 284 eV for carbon.
- Fig. 3 Operation of the rotating crystal spectrometer. The traces are recorded with a Le Croy transient analyzer (ADC 8212P & Memory Module 8800/12). Trace (a) is the "timing" signal from the LED-photodiode combination θ . Trace (b) is the current to the collector plates showing in alternating sequence a spectrum from the TAP and the ADP crystal. The traces further down are on an expanded time scale, exhibiting the characteristic line structure of the iron L-spectrum.
- Fig. 4 Oxygen K-spectrum from PLT.
- Fig. 5 Spectrum of the Ly_{α} - line of hydrogenlike sulfur¹³ showing the splitting of the $^2P_{3/2}$ and $^2P_{1/2}$ level at 4.73Å and also indications of dielectronic satellites at 4.760Å and at 4.784Å.
- Fig. 6 The effect of particle transport on the radial profile of the Ly_{α} radiation. Fig. 6a: Predictions of the density $n_{NeX}(r)$ of hydrogenlike neon for various diffusion coefficients with the MIST code of Hulse and POST¹⁸ Fig. 6b: The corresponding Ly_{α} -profiles.

- Fig. 7 Comparison of the experimentally observed Abel-inverted Ly_{α} profile with theoretical prediction using the MIST code.
- Fig. 8 High resolution spectrum of heliumlike iron measured by Bitter et al.²⁰ The nomenclature of the lines originated from Gabriel¹⁹. w is the main resonance line $1s^2 \ ^1S_0 \rightarrow 1s2p \ ^1P_1$. x and y represent the intercombination lines. z is the forbidden line. t, k, r, and j are $n = 2$ dielectronic satellites. A, B and d_{13} are unresolved $n = 3$ satellites. q and β result from inner shell excitation of lithiumlike and berylliumlike iron.
- Fig. 9 Level diagram of heliumlike ions. Solid arrows represent collisional excitation, dotted arrow radiative transitions. 2ph stands for two photon decay. E1 stands for electric dipole transition, M2 for magnetic quadrupole transition, etc. R, I, F indicate the resonance intercombination and forbidden line.
- Fig. 10 K spectrum of magnesium Mg XI, measured with the rotating crystal spectrometer for $T_{e0} = 1.5$ keV and $n_{e0} = 3 \times 10^{13} \text{ cm}^{-3}$ on PLT.
- Fig. 11 Dielectronic excitation of the $n = 2$ satellite j and the $n = 3$ satellite d_{13} . Radiation less capture of an electron under simultaneous excitation of a bound electron of a heliumlike ion leads to the doubly excited state $1s2p^2 \ ^2D_{5/2}$ of lithiumlike iron. From there the ion can autoionize (the inverse process) or decay by emitting satellite line j. The left part of the figure illustrates which electrons are involved in exciting the resonance line w

(all with energy > 6.7 keV) and the satellite j and $d13$ (only electrons with 4.7 keV or 5.8 keV).

Fig. 12 The line ratio of the dielectronic satellite j to the resonance transition w versus electron temperature (T_e) for iron. The data have been obtained on PLT by Bitter et al.²⁰ The theoretical curves are from Bhalla et al.²⁵ (solid line) and from Bely-Bubau et al.³⁶ (dashed line). The factor α represents the contribution of the unresolved $n \geq 3$ satellites to the intensity of the resonance line.

Fig. 13 K_{α} spectrum of chromium measured by Platz and Ramett²⁷ on TFR, showing satellite lines due to the lithium, beryllium, boron and carbonlike charge state.

Fig. 14 A time sequence of six line profiles of the resonance line w of TiXXI at 2.6099 Å during neutral beam heating (300 ms - 450 ms) on PDX. Solid lines represent least-squares fits by Voigt functions. Arrows indicate the limits used for the fit. The linewidth increases due to Doppler broadening and the line center shift to shorter wavelength due to toroidal rotation.

Fig. 15 Calculated contribution of the unresolved $n \geq 3$ dielectronic satellites to the resonance line w (dashed curve) for iron according to Bely-Dubau et al.³⁶

Fig. 16 Comparison of theoretical predictions³⁶ (I) for the line profile of the resonance line w (II) and the unresolved $n \geq 3$ satellites (III)

with the experimental lineshape by Bitter et al.²⁴ To obtain agreement it was necessary to increase the theoretical wavelength of the $n = 3$ satellites by $\Delta\lambda = .0003 \text{ \AA}$.

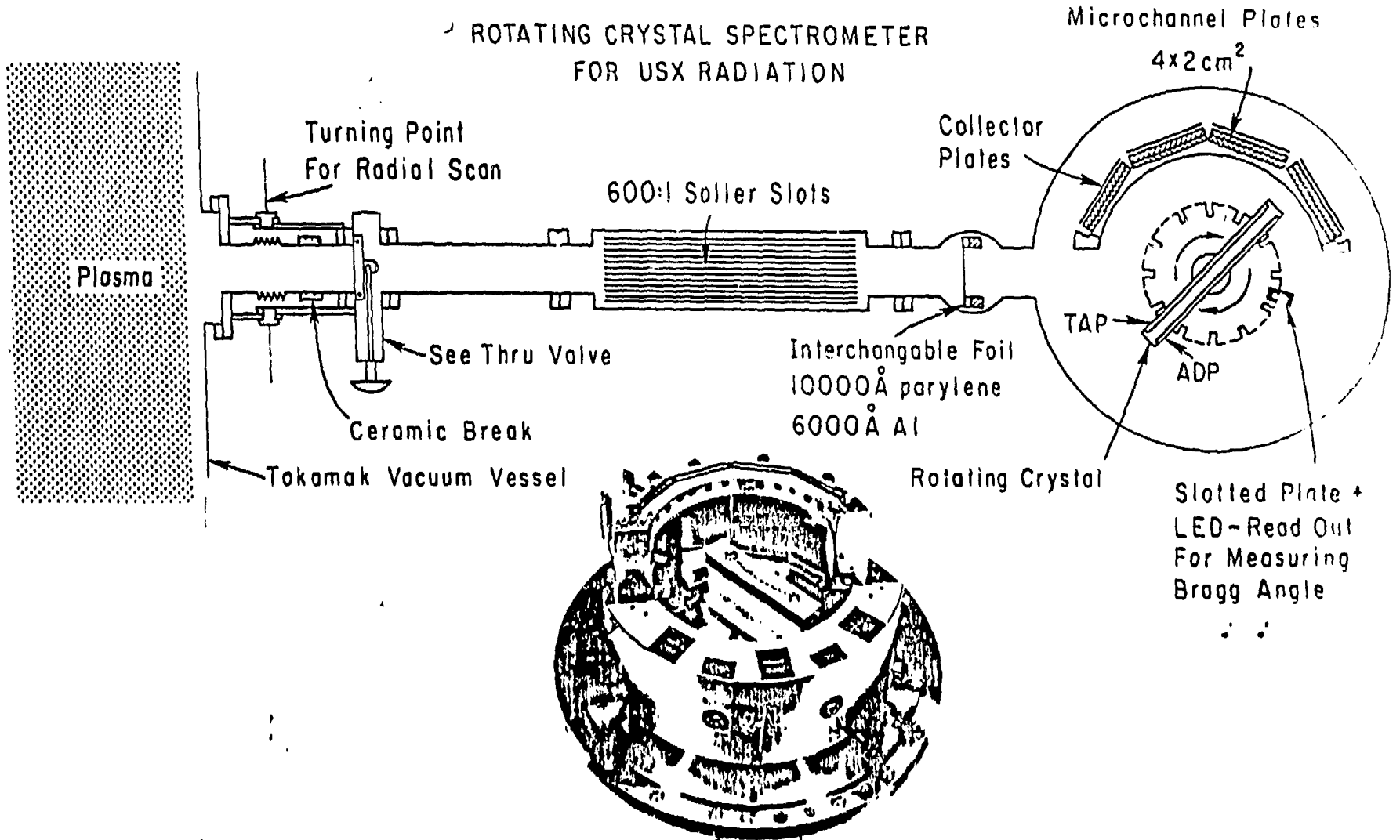
Fig. 17 The L spectrum of stainless steel measured with the rotating crystal spectrometer on PLT. Most of the transitions are due to iron and the transition type has been indicated above the spectrum.

Fig. 18 Radial profiles of the chord integrated intensity of the most prominent iron L lines.

Fig. 19 Titanium L spectrum obtained with the rotating crystal spectrometer on PLT using laser blowoff techniques²¹. The lithium like TiXX lines are indicated by arrows.

Fig. 20 Germanium L spectrum obtained with the rotating crystal spectrometer on PLT using laser blow off techniques²¹. The neonlike transitions are indicated by arrows.

ROTATING CRYSTAL SPECTROMETER
FOR USX RADIATION

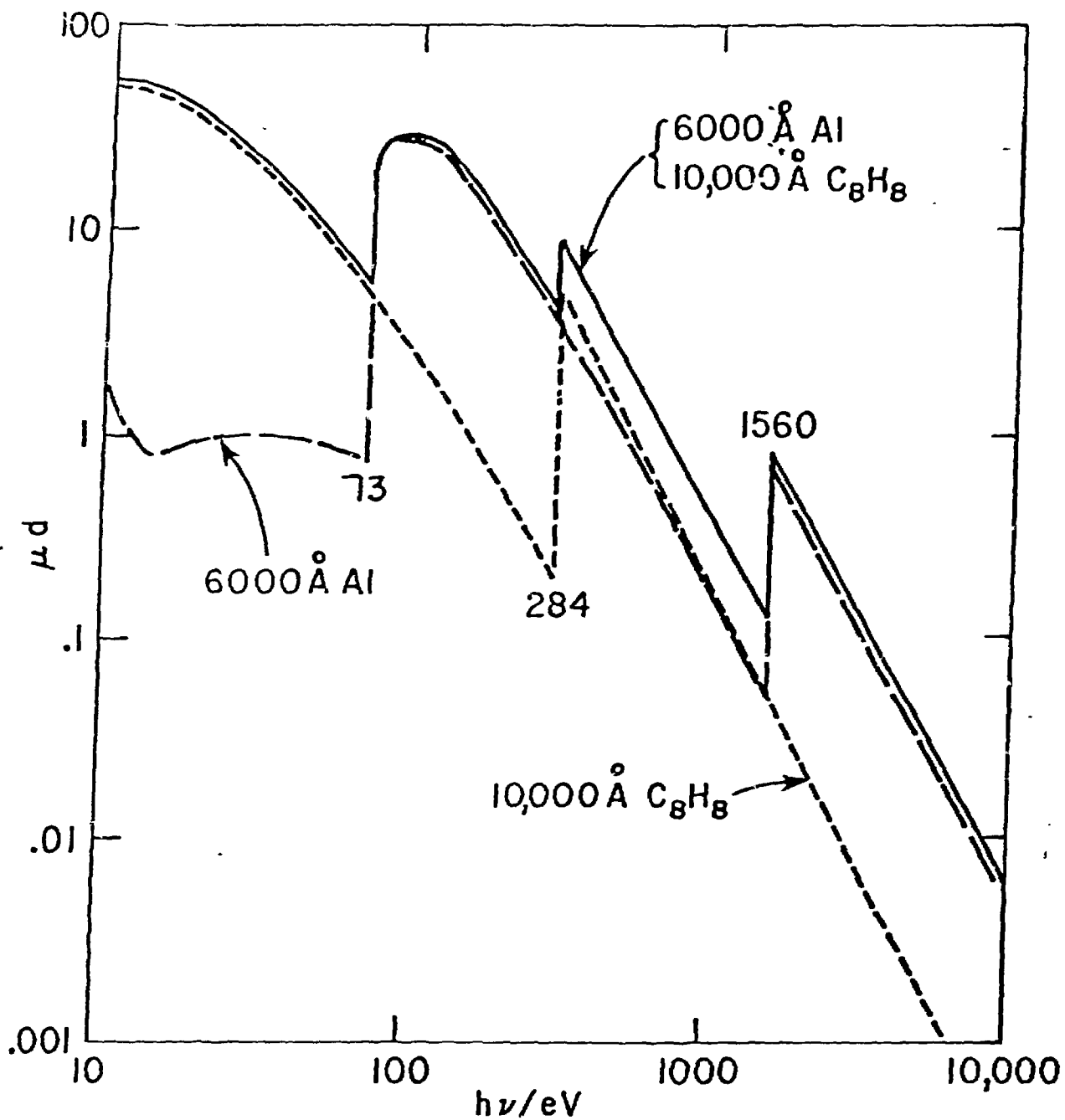


← 6" wide →

Fig. 1

80 90 45

ABSORPTION OF AL AND PARYLENE

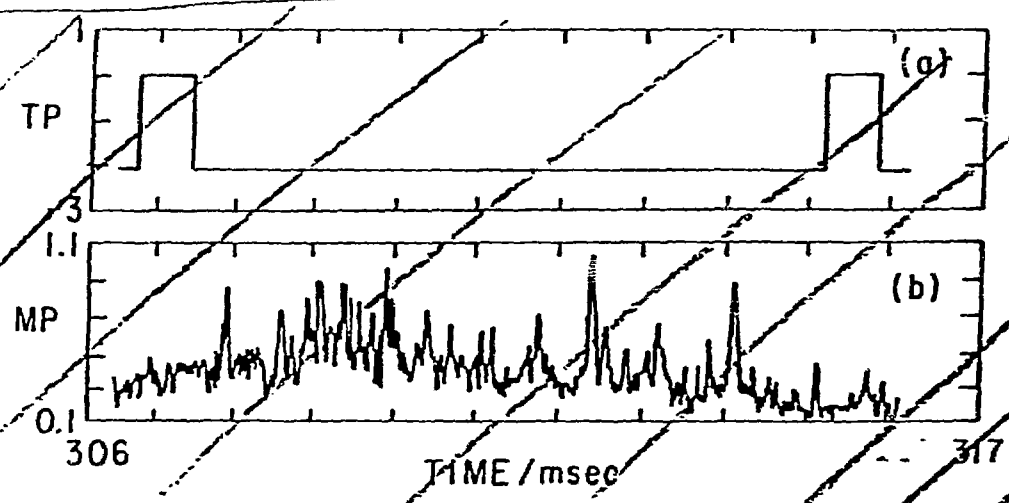
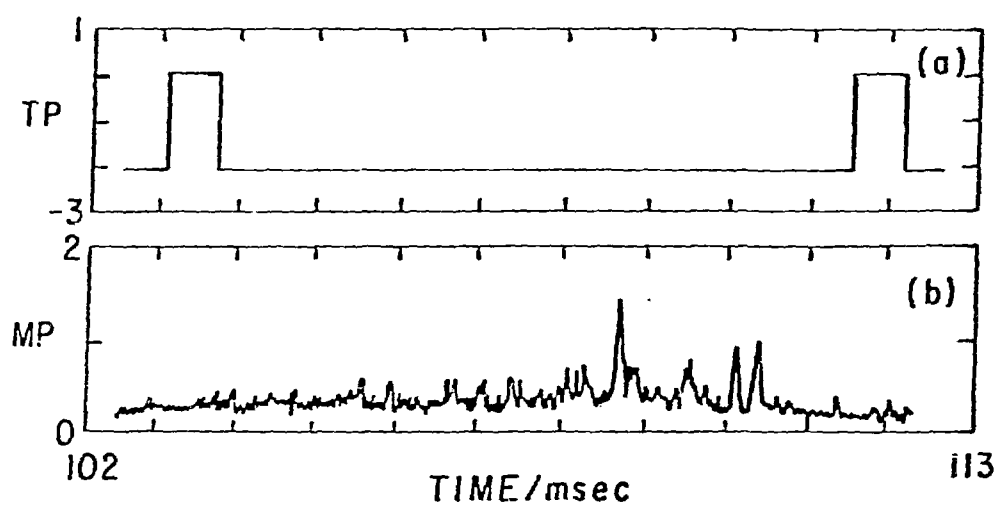
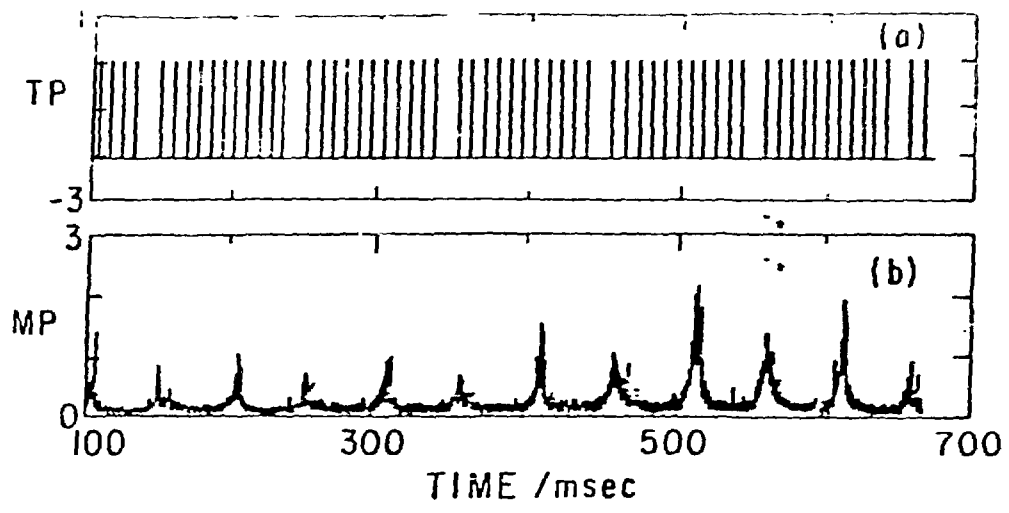


with Berovic

3" wide

Fig. 2

~~5067-28~~



$3\frac{1}{2}$ " wide

80 90 56

Fig. 3

82X0649

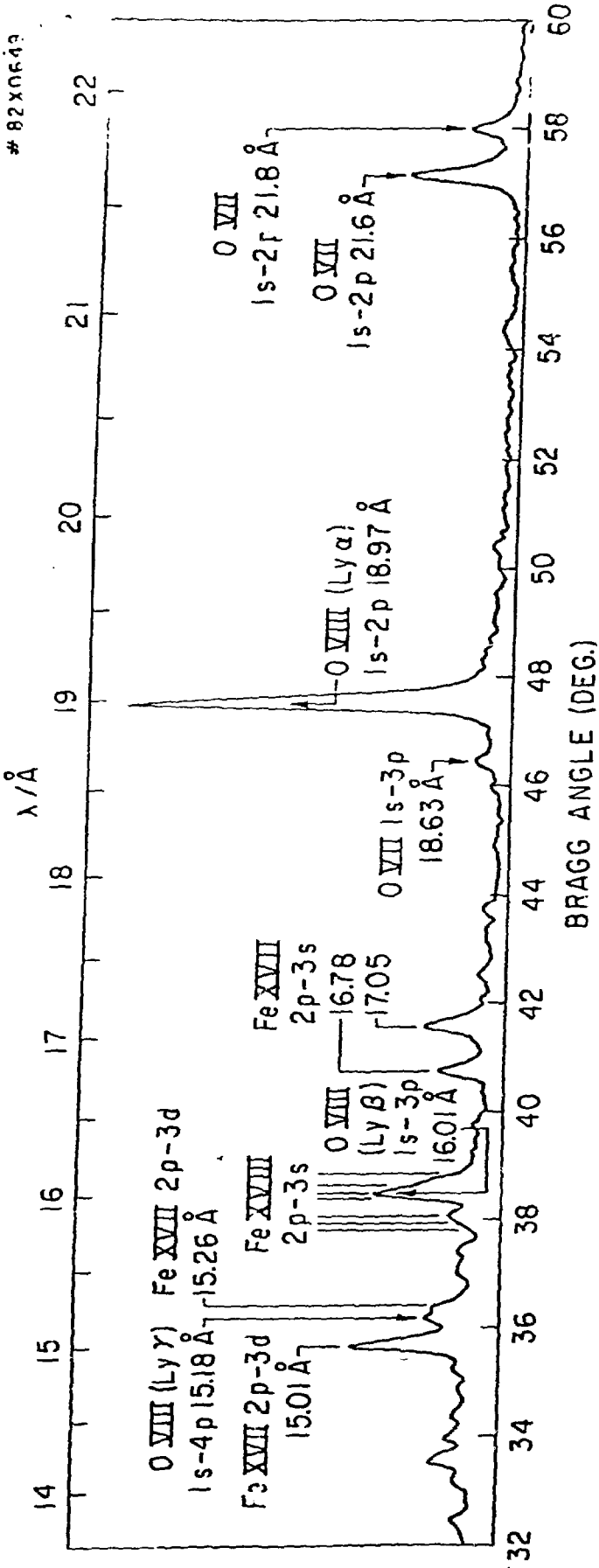
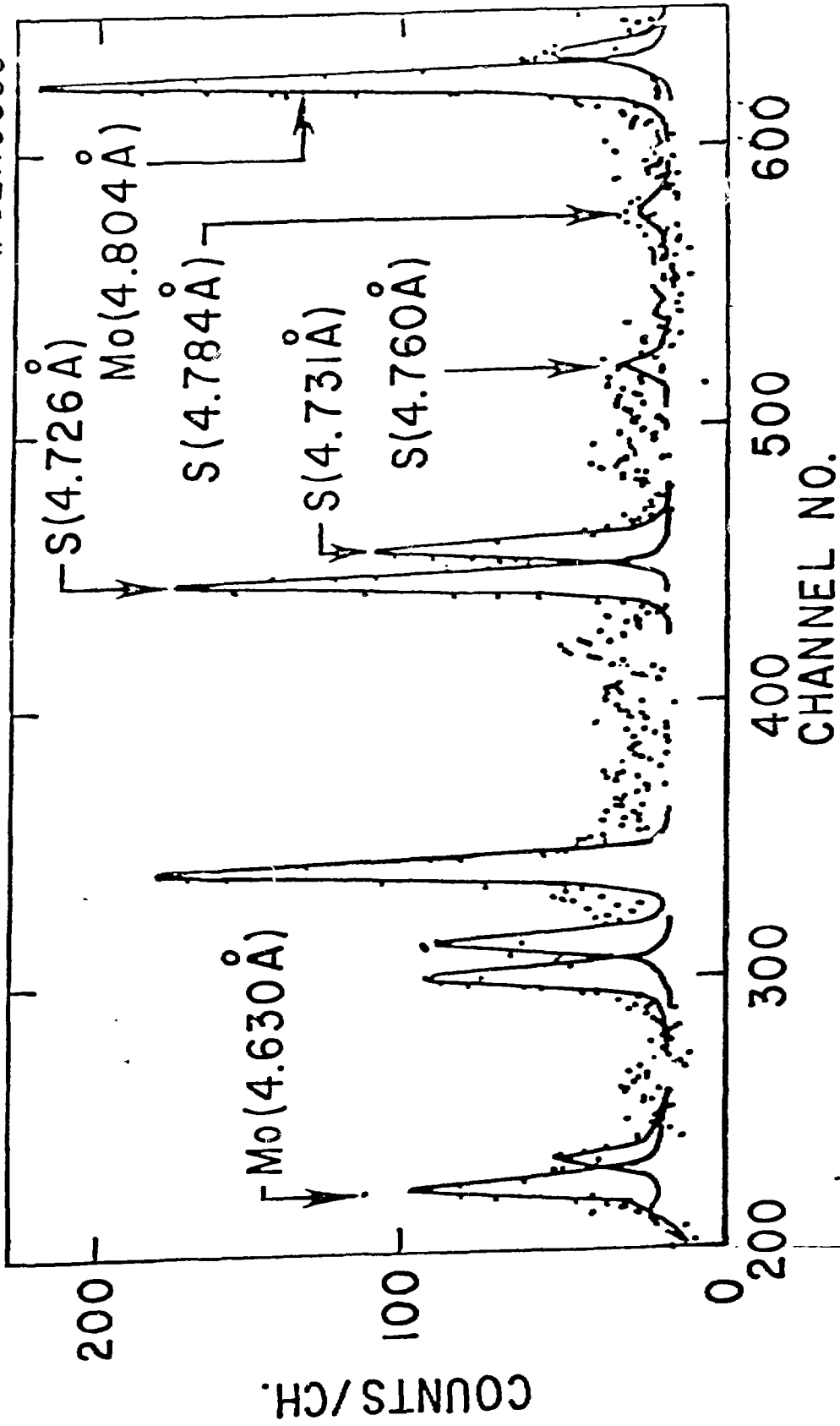


Fig. 4

6" wide

#82X0605



← 4.5" wide →

Fig. 5

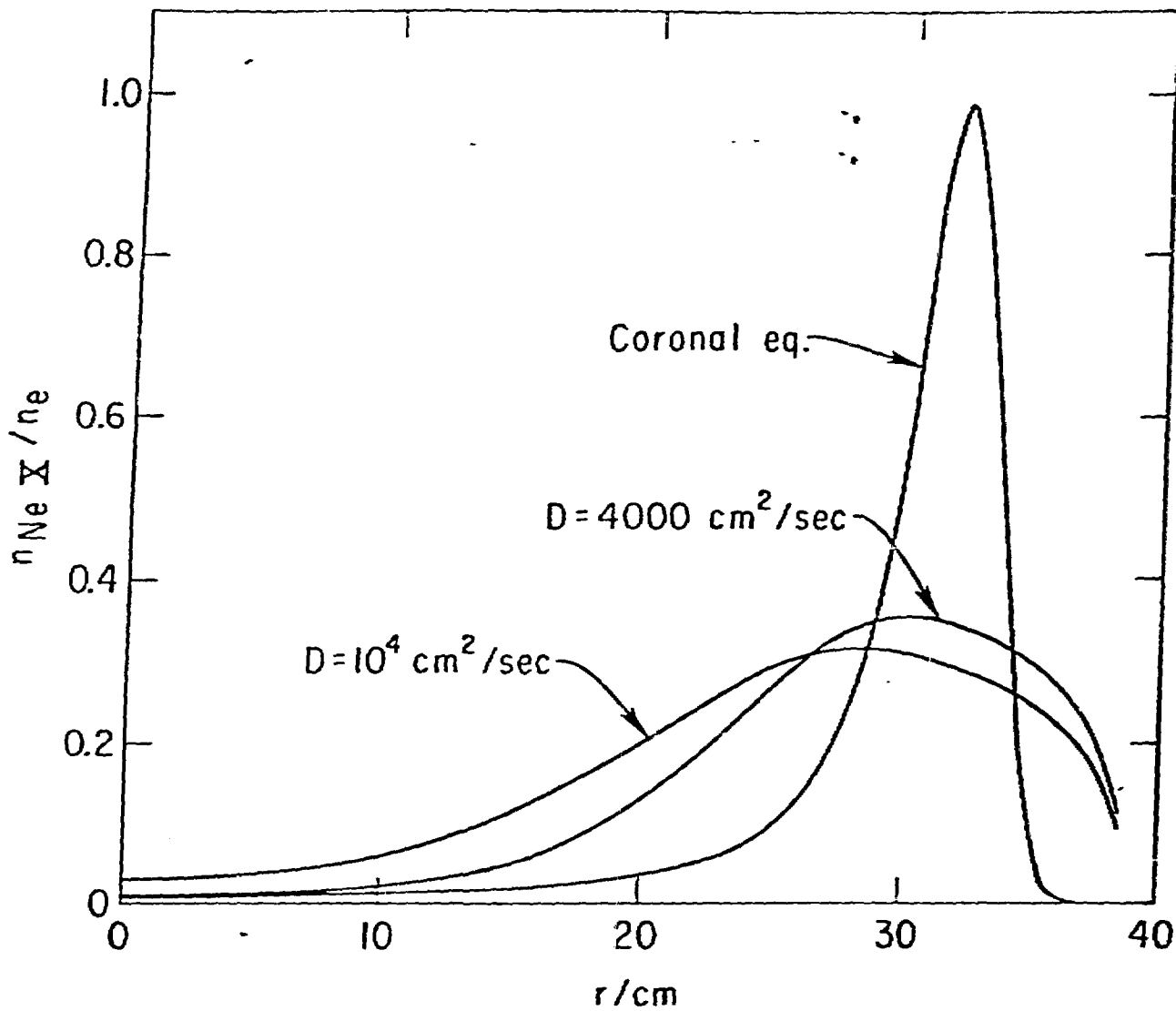


Fig. 6a

↔ 3 1/2" wide →

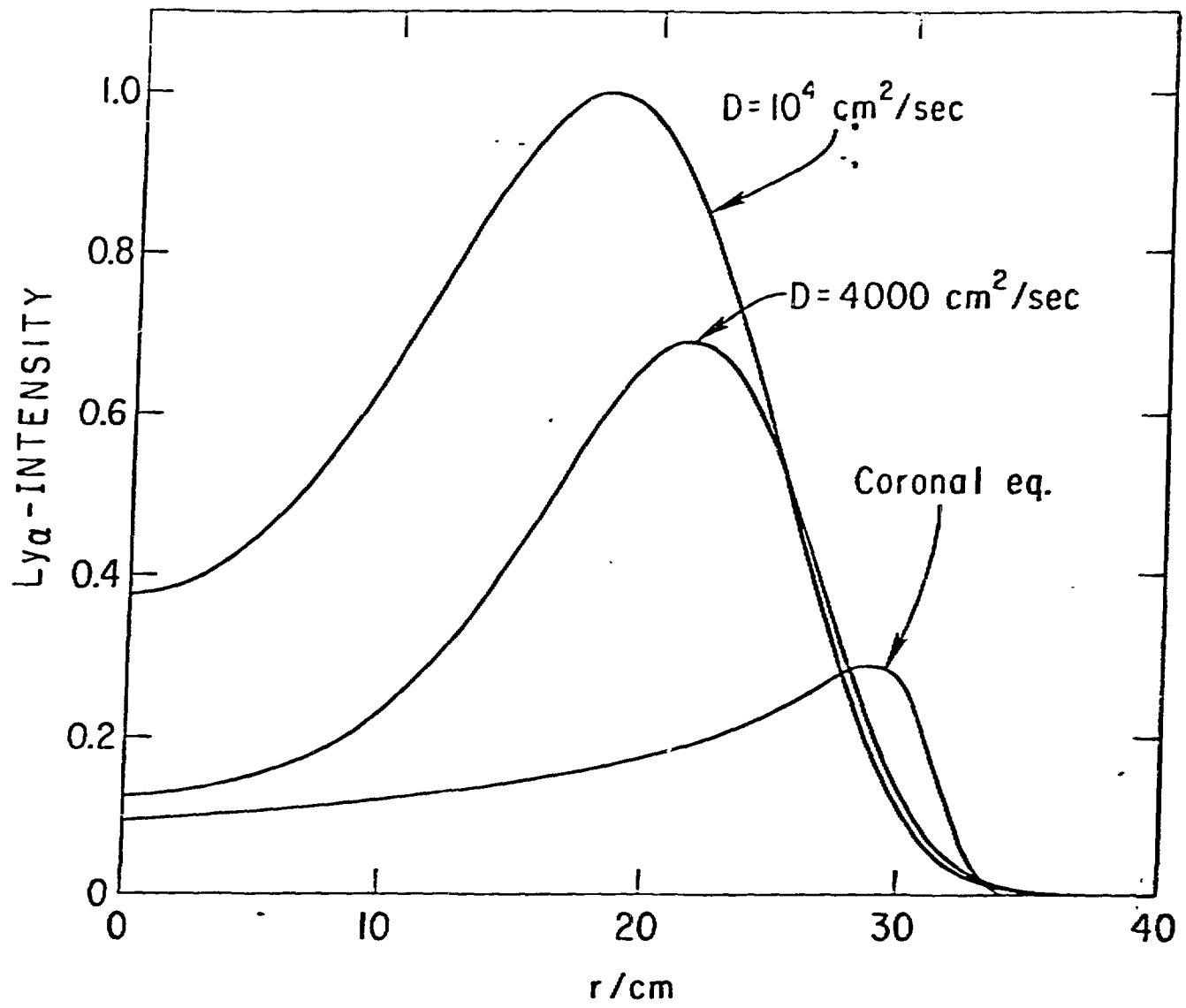
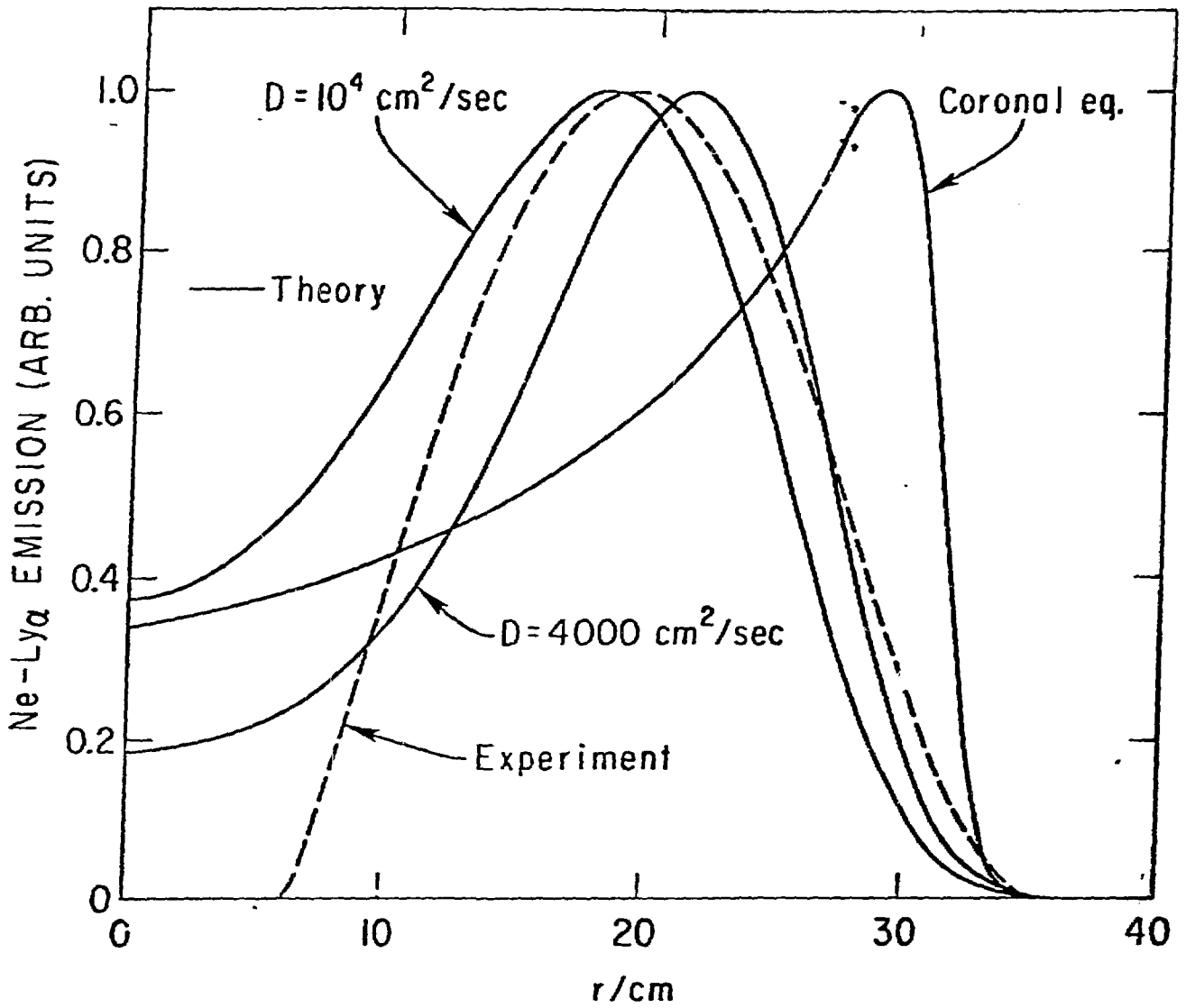


Fig. 6B (put below Fig 6a?)

3 1/2" wide

Size should be equal to Fig 6a !!



$\leftarrow 3\frac{1}{2}'' \text{ wide} \rightarrow$

Fig. 7

82 X 0672

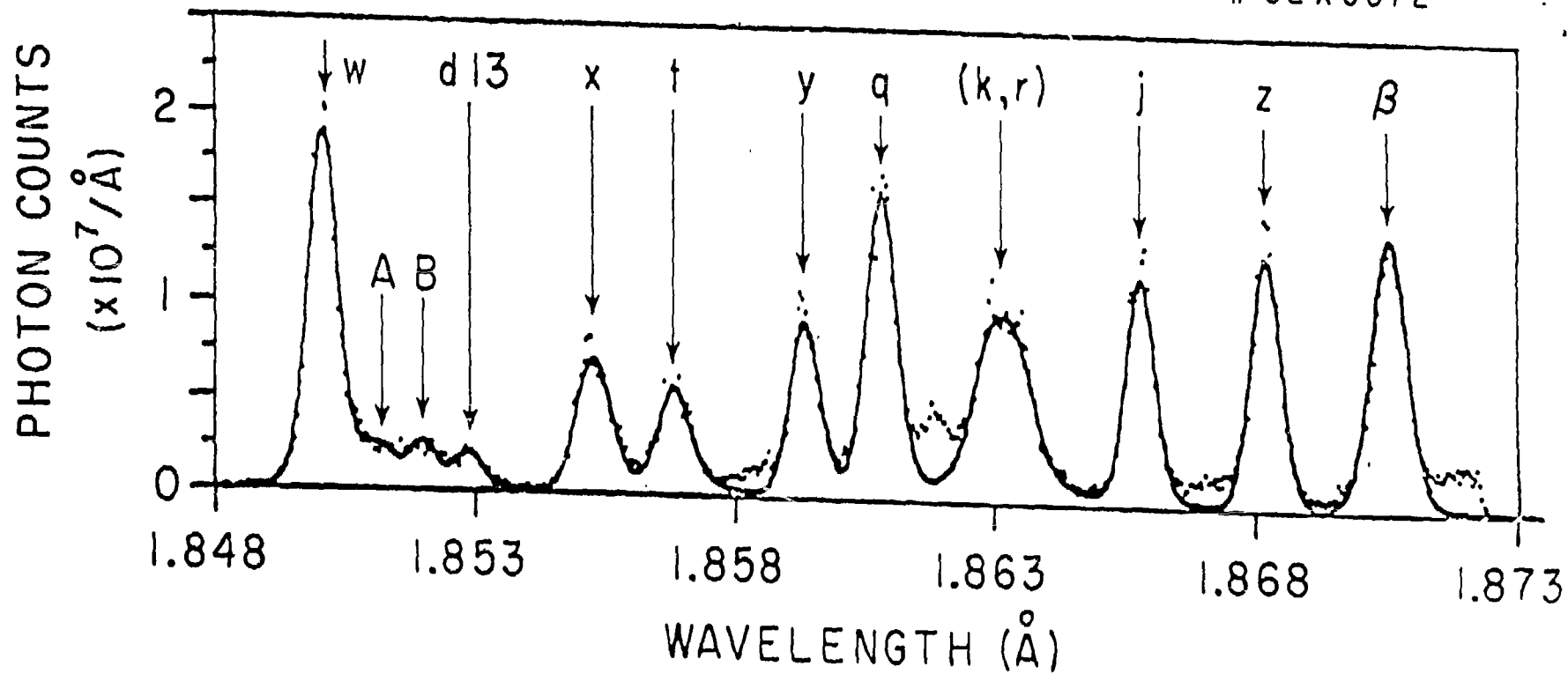
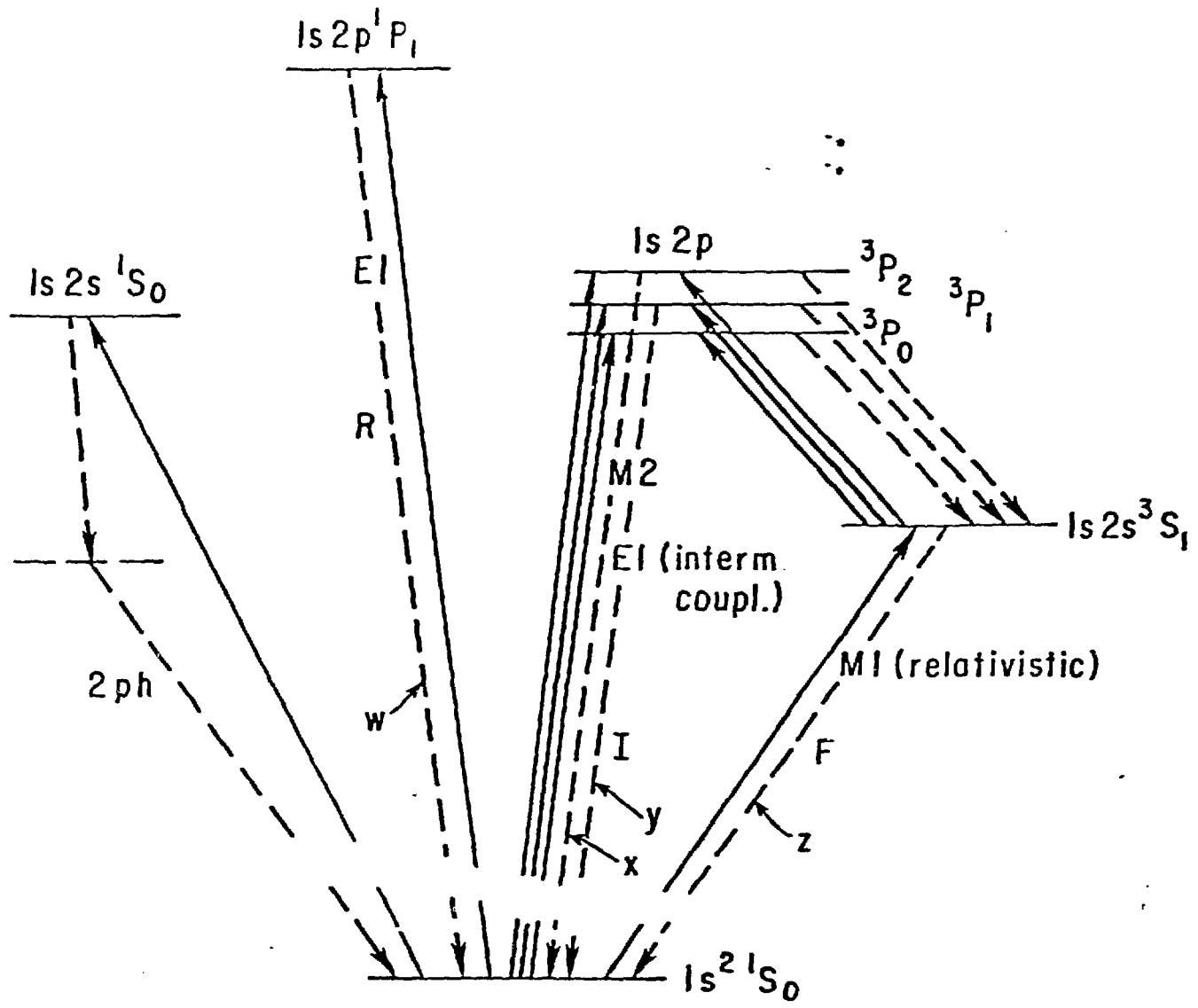


Fig. 8.

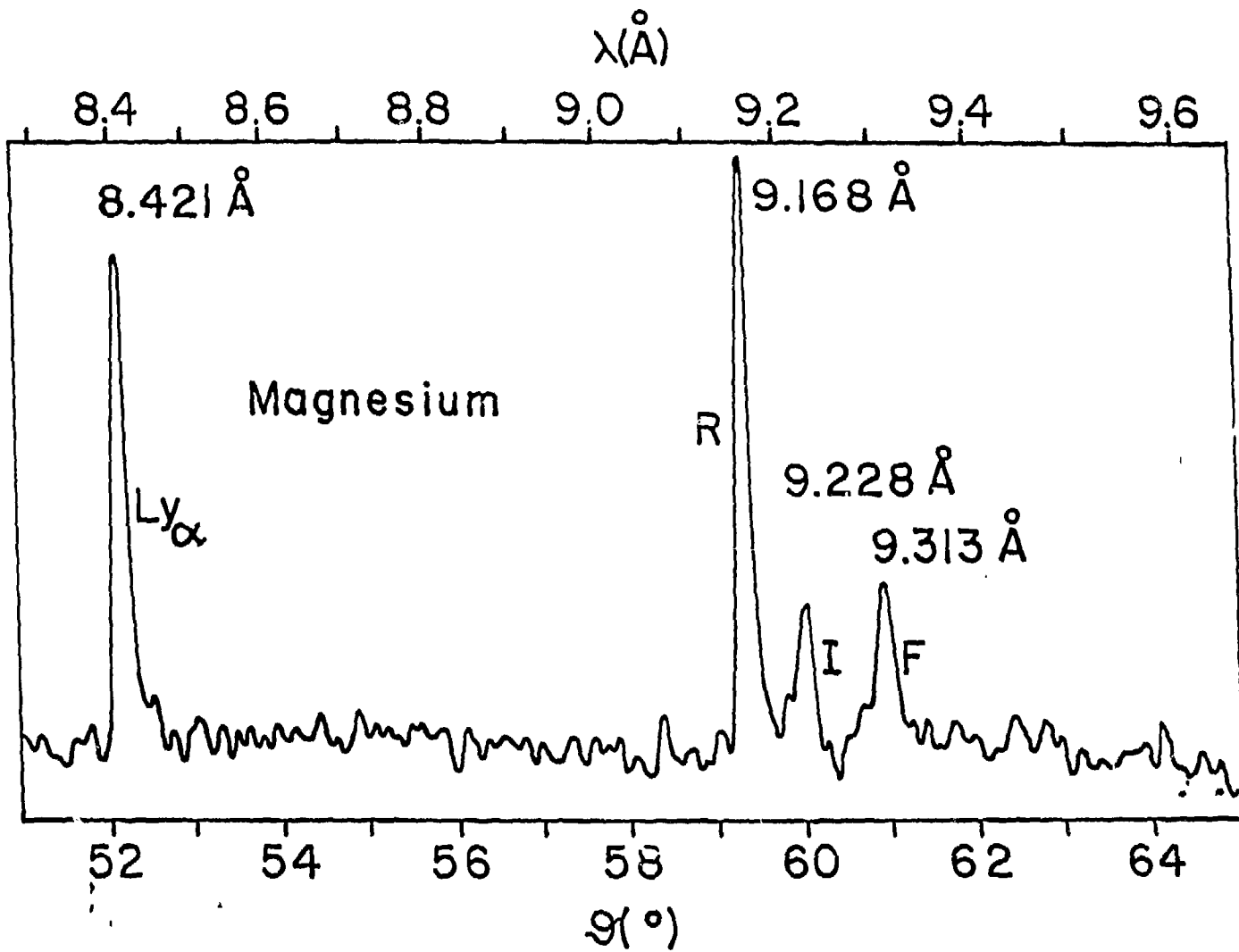
$\leftarrow 4\frac{1}{2}'' \text{ wide} \rightarrow$



← 3'' →

Fig. 9

Fig. 10
a.p.f



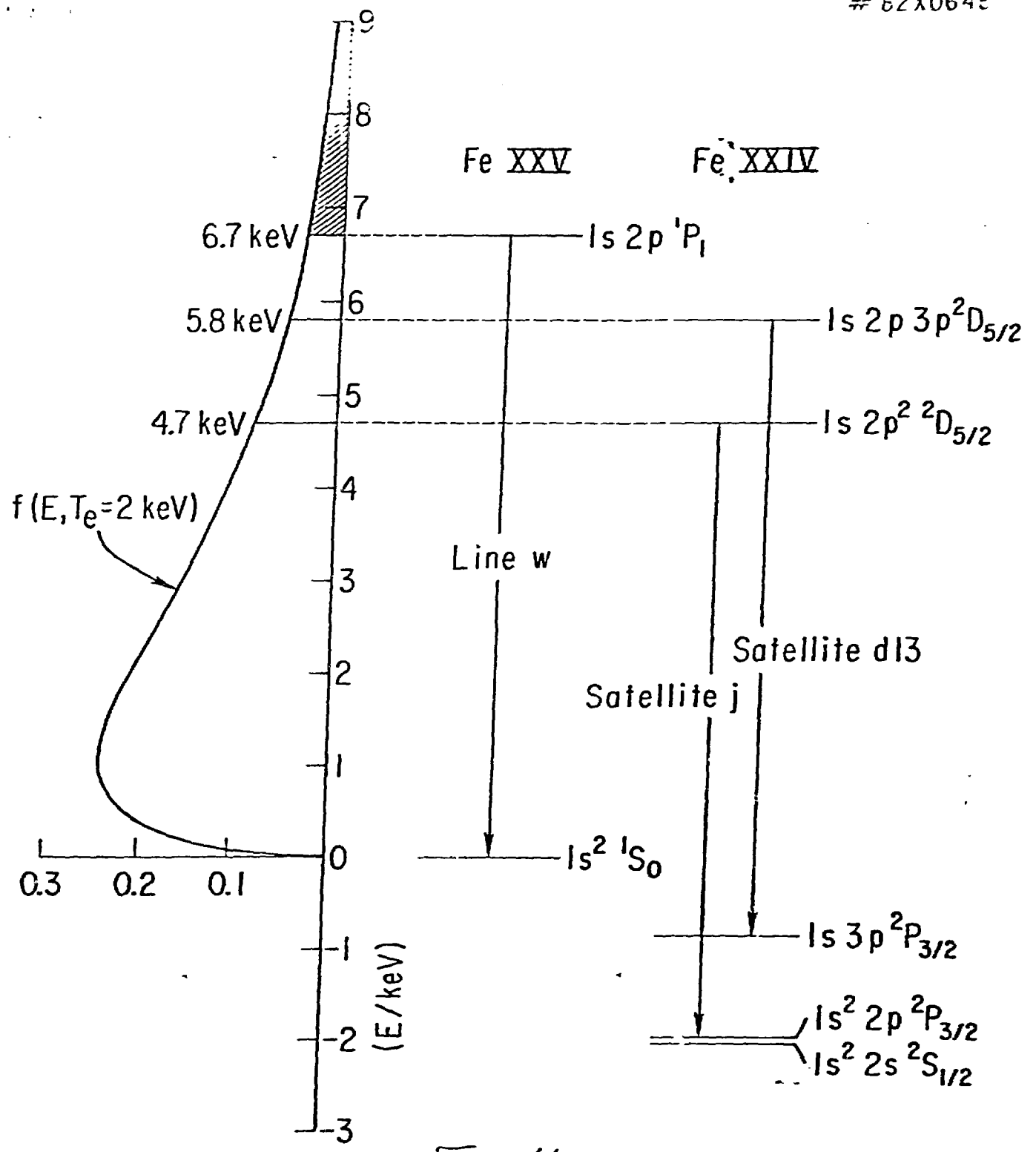
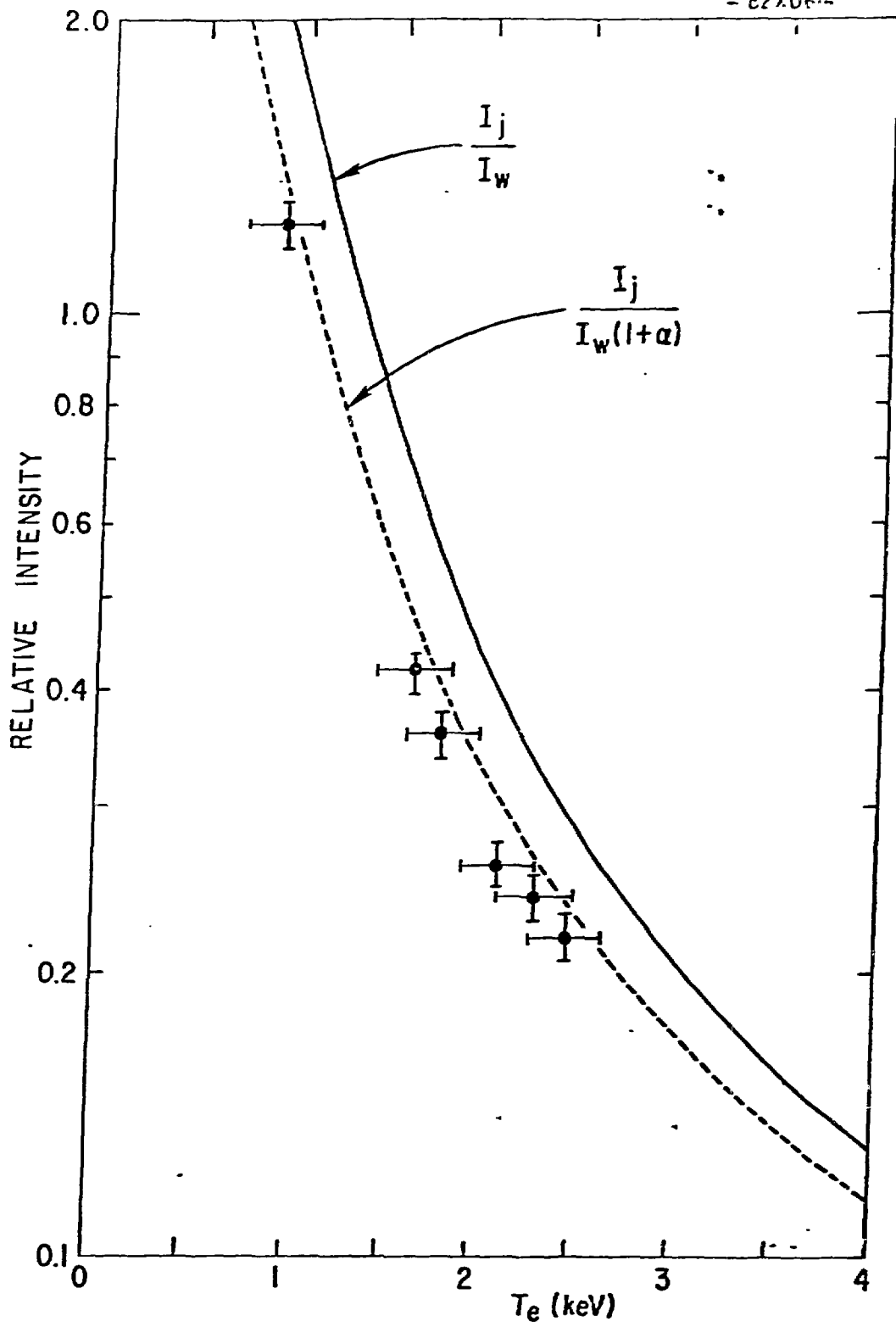


Fig. 11

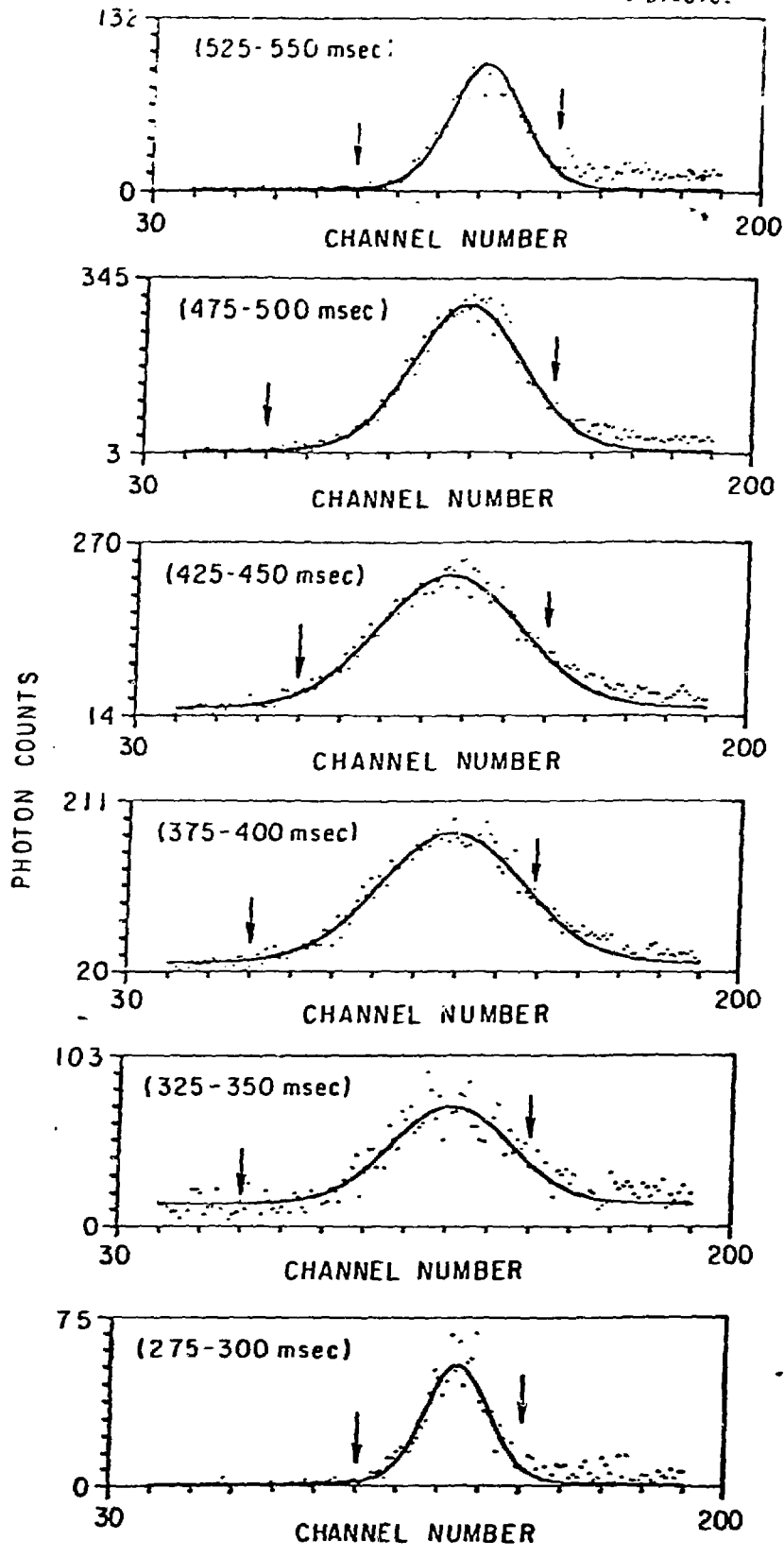
~~Fig. 11~~

$3 \frac{1}{2}^4$ wide \rightarrow



← 4'' →

Fig. 12



$\sigma \approx 3\frac{1}{4}$ wide \rightarrow

~~Fig. 14~~ Fig. 14

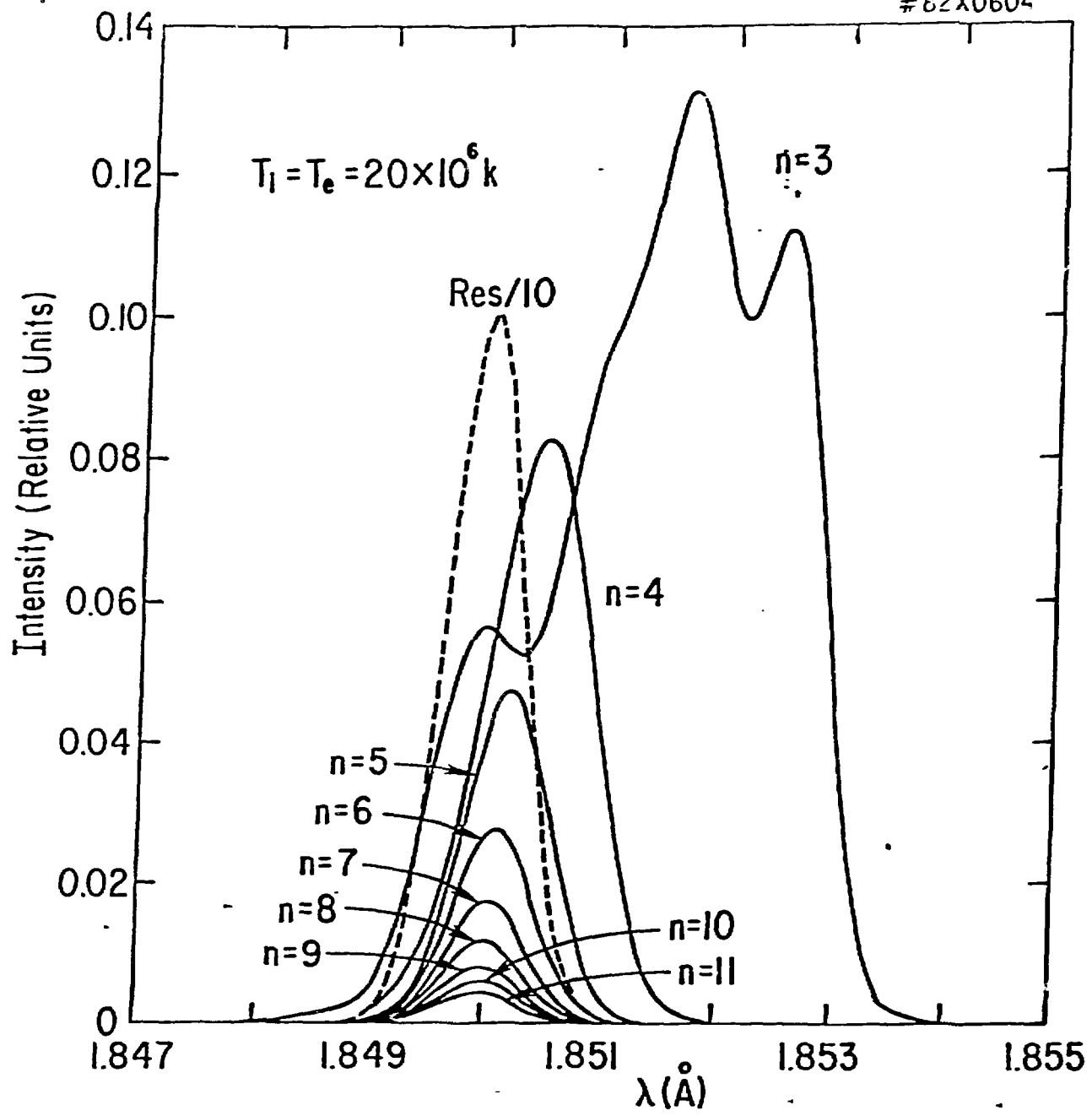
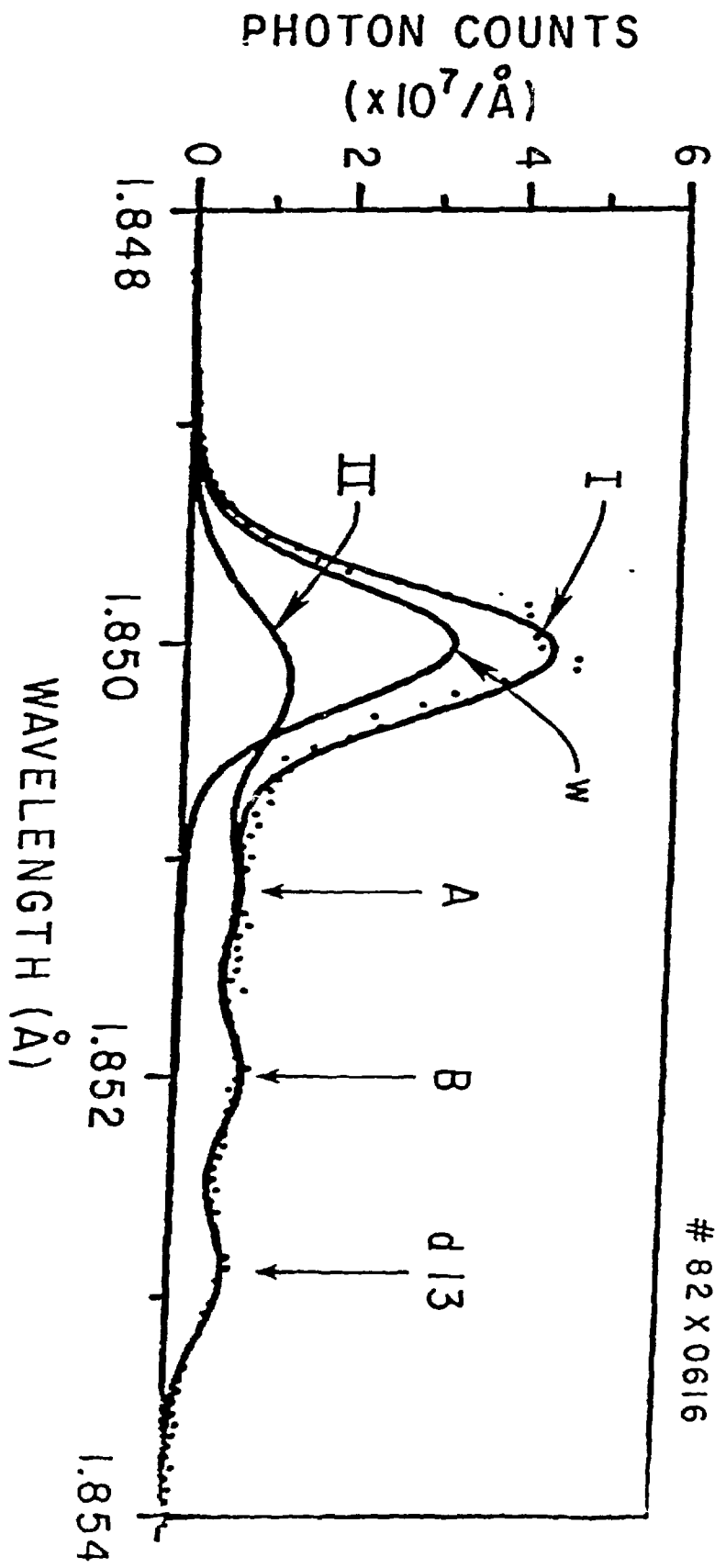


Fig. 15

← 4 " wide →

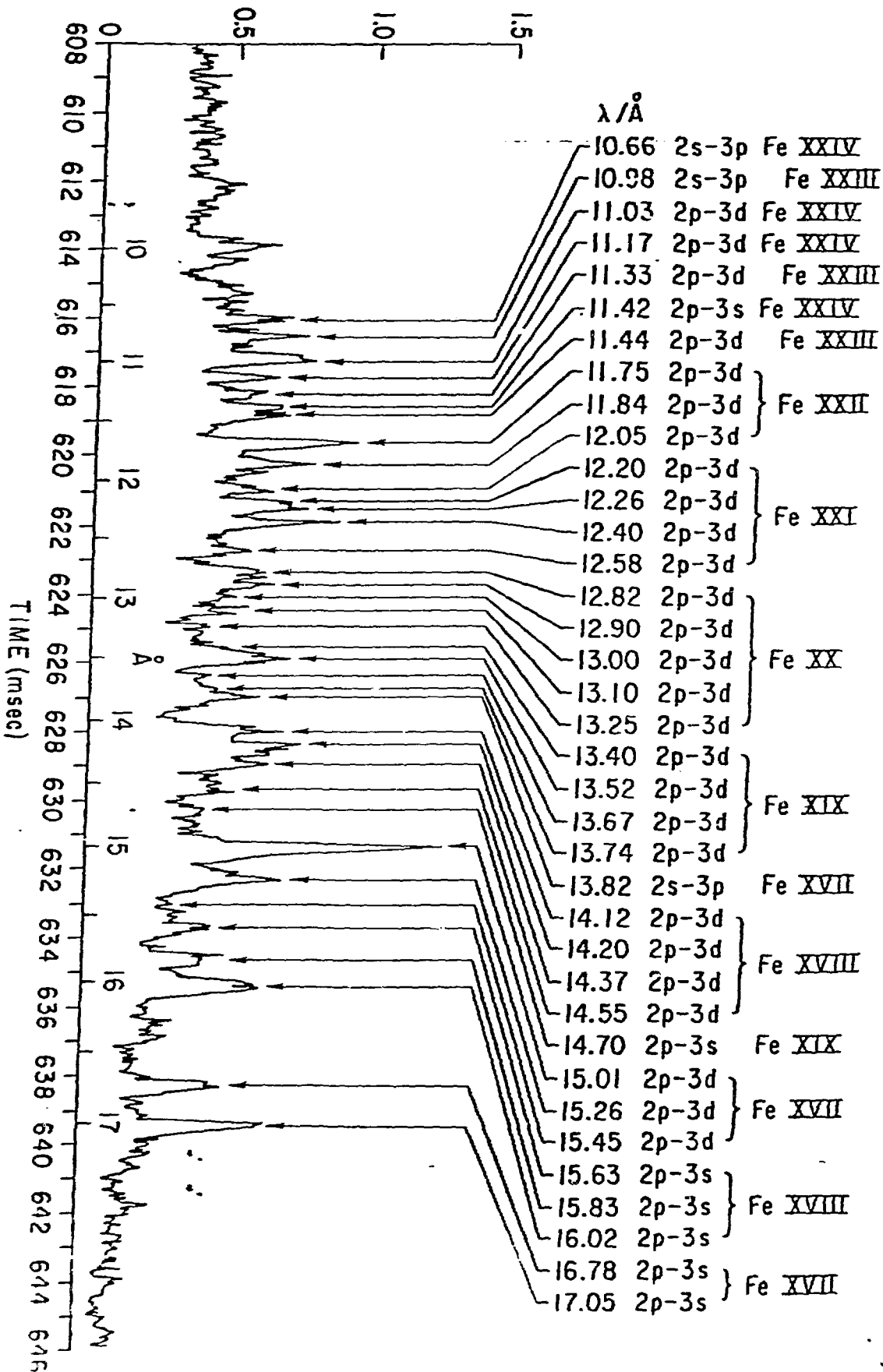


82 X 0616

Fig. 16

4.0" wide →

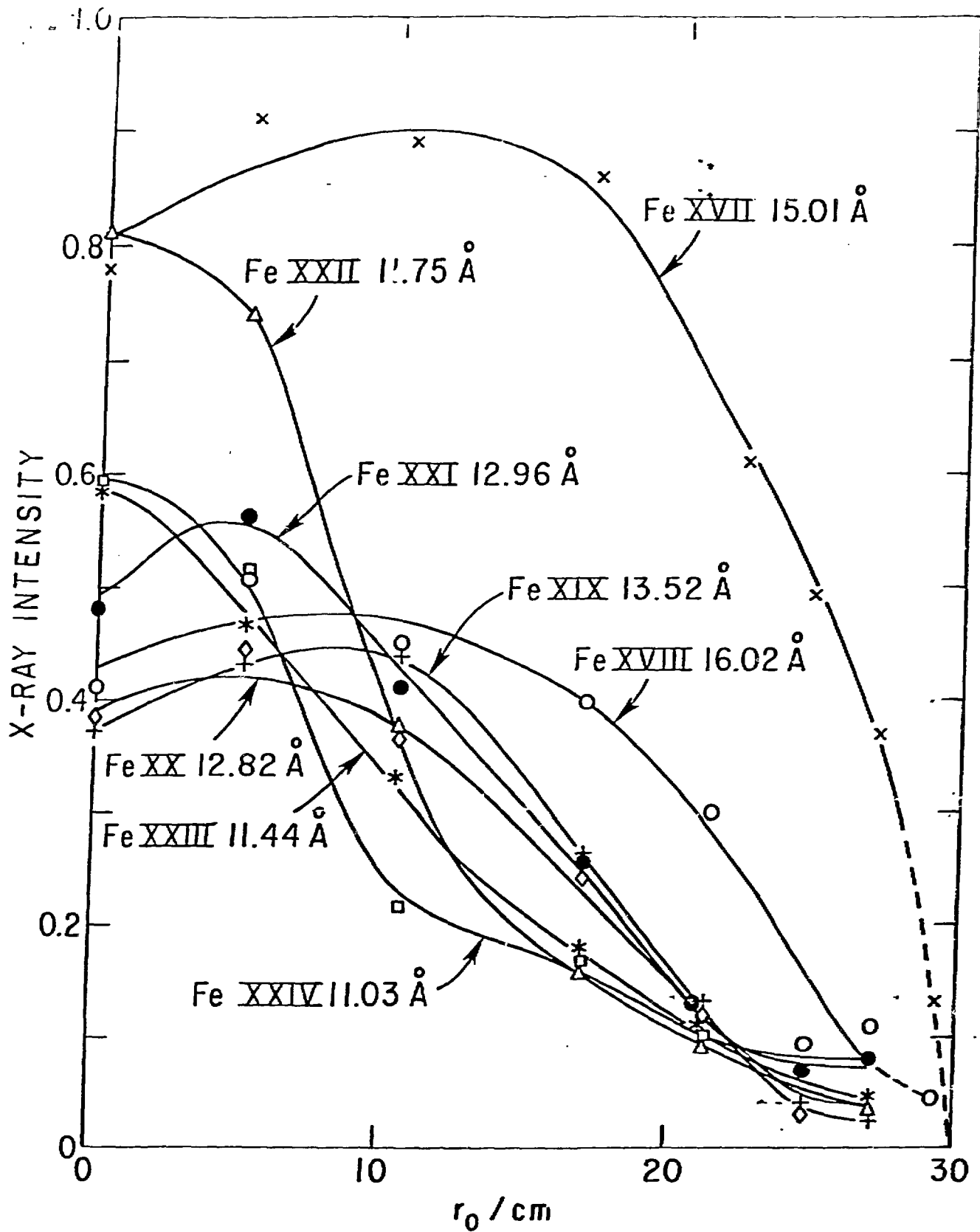
X-RAY INTENSITY



6" wide

Fig. 17

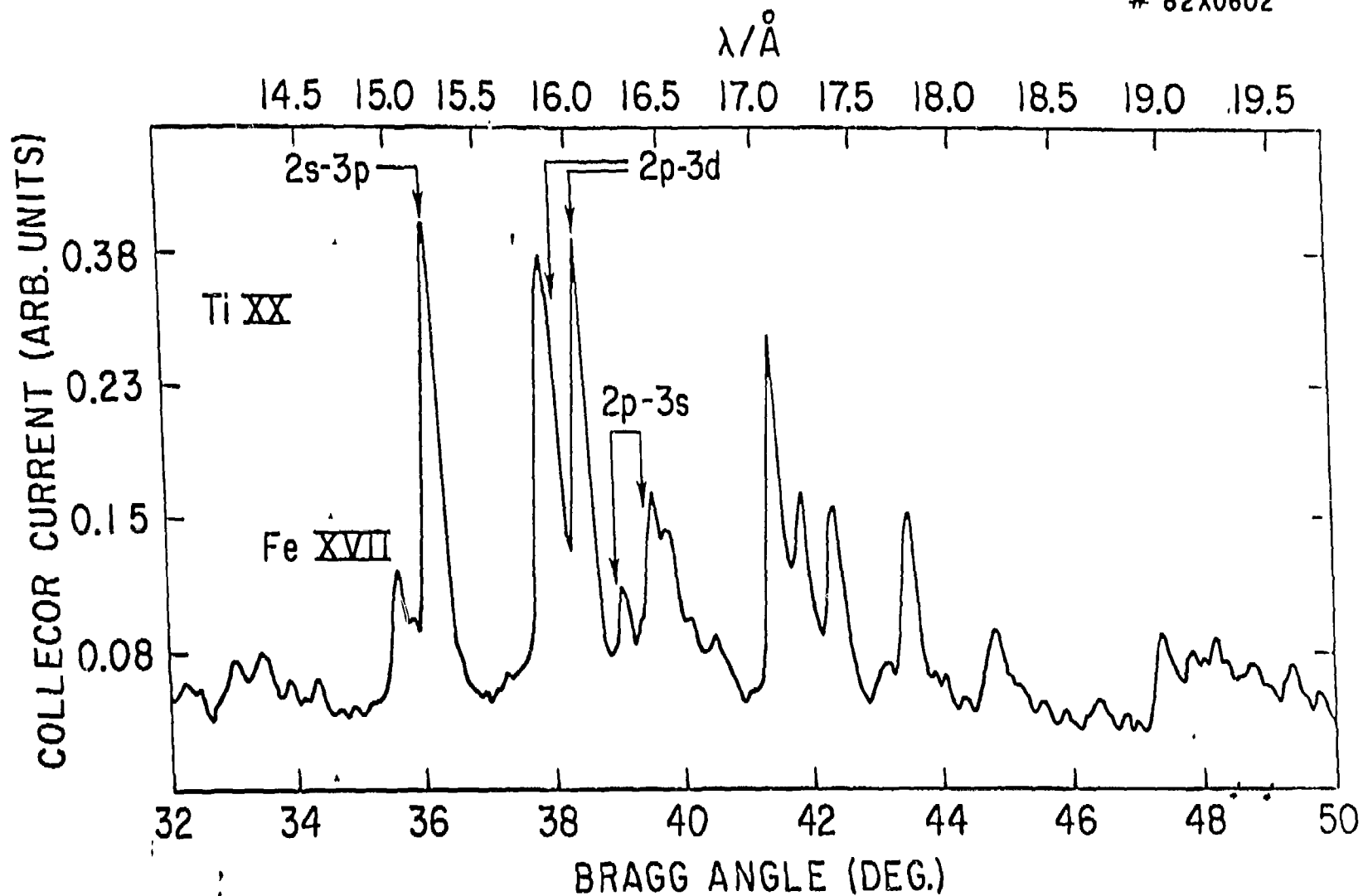
80 67 47



← 4" →

Fig. 18

806748



← 4.5 " →

Fig. 19

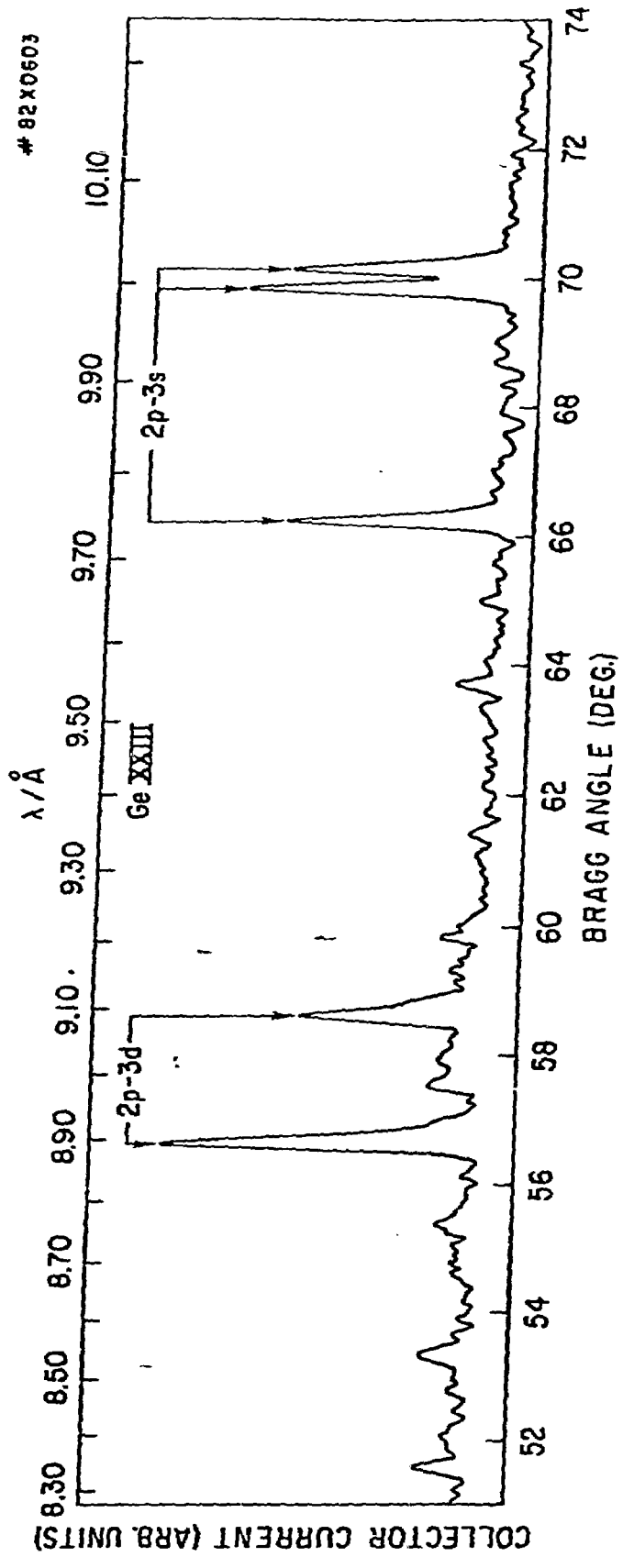


Fig. 20